
Improving Fine-Grained Control via Aggregation of Multiple Diffusion Models

Conghan Yue
Sun Yat-Sen University

Zhengwei Peng
Sun Yat-Sen University

Shiyan Du
Sun Yat-Sen University

Zhi Ji
University of Toronto

Chuangjian Cai
Game AI Center, Tencent

Le Wan
Game AI Center, Tencent

Dongyu Zhang *
Sun Yat-Sen University

Abstract

While many diffusion models perform well when controlling for particular aspect among style, character, and interaction, they struggle with fine-grained control due to dataset limitations and intricate model architecture design. This paper first introduces a novel training-free algorithm in fine-grained generation, Aggregation of Multiple Diffusion Models (AMDM), which integrates features from multiple diffusion models into a specified model to activate specific features and enable fine-grained control. Experimental results demonstrate that AMDM significantly improves fine-grained control without training, validating its effectiveness. Additionally, it reveals that diffusion models initially focus on features such as position, attributes, and style, with later stages improving generation quality and consistency. AMDM offers a new perspective for tackling the challenges of fine-grained conditional control generation in diffusion models: We can fully utilize existing or develop new conditional diffusion models that control specific aspects, and then aggregate them using AMDM algorithm. This eliminates the need for constructing complex datasets, designing intricate model architectures, and incurring high training costs. Code is available at: <https://github.com/Hammour-steak/AMDM>.

1 Introduction

Diffusion models [1, 2, 3, 4, 5] have achieved excellent performance in generative tasks. In particular, conditional diffusion models [6, 7, 8] not only deliver advanced results in practical applications such as Text-to-Image [9, 10, 11, 12] and Image-to-Image generation [13, 14], but also offer highly flexible conditional control mechanisms.

Recent research on conditional diffusion models has focused on achieving fine-grained control, including object attributes [15, 16], interactions [17, 18], layouts [19, 20, 21], and style [22, 23, 24]. However, maintaining consistency across diverse nuanced control remains a significant challenge. Generating multiple objects with overlapping bounding boxes can lead to attribute leakage, where the description of one object inappropriately influences others, causing inconsistencies between objects and the background. Fine-grained interaction details may be illogical, and style integration may compromise object attributes.

*Corresponding Author

Existing approaches only partially address these issues due to the inherent complexity and diversity of fine-grained control, coupled with limitations in datasets and model architectures. Some works [25, 26, 27] may perform well in preventing attribute leakage among multiple instances during layout generation but perform poorly in managing object interactions, while others [28, 23] may excel in style transfer but exhibit limited control over layout.

Interestingly, most of these methods are based on Stable Diffusion [6], which is theoretically grounded in DDPM [2] and classifier-free guidance [29] for conditional control. Therefore, for these conditional diffusion models that are grounded in the same theoretical foundation, our objective is to overcome this challenge by developing a method that effectively aggregates the advantages of each model, leveraging their unique strengths to achieve fine-grained control.

This paper proposes a novel algorithm called Aggregation of Multiple Diffusion Models (AMDM). It aggregates intermediate variables from different conditional diffusion models which based on the same theoretical foundation, into a specific model during inference. This approach enhances features by absorbing characteristics from different models, regardless of variations in architecture or training datasets, without requiring additional training, avoiding the need for complex datasets and intricate model designs. Our experiments show that our proposed algorithm AMDM significantly improves the fine-grained generation capability of a specific conditional diffusion model. Furthermore, it demonstrates that diffusion models with a shared theoretical foundation allowing operations on their intermediate variables, while also revealing a phenomenon where early sampling steps focus on generating diverse features, and later stages prioritize quality and consistency.

Our main contributions are as follows:

- We propose a novel diffusion model aggregation algorithm, AMDM, that can aggregate intermediate variables from different conditional diffusion models of the same diffusion process, absorbing the characteristics of each model and enabling fine-grained generation.
- We conduct a variety of experiments, and both visual and quantitative results demonstrate noticeable improvements in areas where the models previously exhibited weaker control, validating the effectiveness of AMDM.
- AMDM reveals that diffusion models initially focus on generating features like position, attributes, and style, while later stages emphasize quality and consistency. This allows aggregation algorithms to be used only in the first s steps, significantly reducing computational overhead.

2 Preliminaries

2.1 Diffusion Models

Diffusion models are a class of generative models that progressively add noise to guide the data distribution $q(\mathbf{x}_0)$ towards a Gaussian distribution. In the classical DDPM [2] formulation, the noise addition process from time $t - 1$ to t is defined as:

$$q(\mathbf{x}_t | \mathbf{x}_{t-1}) = \mathcal{N}(\sqrt{\alpha_t} \mathbf{x}_{t-1}, (1 - \alpha_t) \mathbf{I}), \quad (1)$$

where, \mathbf{x}_t represents the noisy data at timestep $t \in [0, T]$, α_t is the coefficient drift schedule generally satisfying $\lim_{t \rightarrow T} \alpha_t = 0$. From (1), we can readily derive the forward marginal distribution:

$$q(\mathbf{x}_t | \mathbf{x}_0) = \mathcal{N}(\sqrt{\bar{\alpha}_t} \mathbf{x}_0, (1 - \bar{\alpha}_t) \mathbf{I}), \quad (2)$$

where $\bar{\alpha}_t = \prod_{i=1}^t \alpha_i$. Equation (2) indicates that we can directly obtain \mathbf{x}_t from \mathbf{x}_0 avoiding multistep sampling. Assuming the generative model is $p_\theta(x_0)$, consider the variational lower bound of its likelihood as the loss function, i.e., the KL divergence of the joint probability:

$$\mathcal{L} = KL(q(\mathbf{x}_{0:T}) || p_\theta(\mathbf{x}_{0:T})) \propto \mathbb{E}_{t, \mathbf{x}_t, \epsilon_t} [\|\epsilon_t - \epsilon_\theta(\mathbf{x}_t, t)\|^2], \quad (3)$$

where $\epsilon_t \sim \mathcal{N}(\mathbf{0}, \mathbf{I})$ and $\epsilon_\theta(\mathbf{x}_t, t)$ is the denoising neural network. More generally, we utilize DDIM [3] sampling which directly defines the forward process (2) compared to DDPM. Ultimately, the reverse sampling process as follows:

$$p_\theta(\mathbf{x}_{t-1} | \mathbf{x}_t) = \mathcal{N} \left(\sqrt{\frac{\bar{\alpha}_{t-1}}{\bar{\alpha}_t}} \mathbf{x}_t + \left(\sqrt{1 - \bar{\alpha}_{t-1} - \sigma_t^2} - \sqrt{\frac{\bar{\alpha}_{t-1}(1 - \bar{\alpha}_t)}{\bar{\alpha}_t}} \right) \epsilon_\theta(\mathbf{x}_t, t), \sigma_t^2 \mathbf{I} \right), \quad (4)$$

where σ_t is a free variable. When $\sigma_t^2 = \frac{1-\bar{\alpha}_{t-1}}{1-\bar{\alpha}_t}(1 - \frac{\bar{\alpha}_t}{\bar{\alpha}_{t-1}})$, it corresponds to DDPM sampling, while $\sigma_t^2 = 0$ results in a deterministic sampling, which is the origin of the name DDIM.

2.2 Classifier-Free Guidance

The key of conditional control in diffusion models is estimating $q(\mathbf{x}_{t-1}|\mathbf{x}_t, y)$ given the condition y . In unconditional generation, according to (4), it can be written as:

$$p_\theta(\mathbf{x}_{t-1} | \mathbf{x}_t) = \mathcal{N}(\boldsymbol{\mu}_\theta(\mathbf{x}_t, t), \sigma_t^2 \mathbf{I}). \quad (5)$$

Accordingly, Classifier-Free Guidance [29] directly incorporates the condition y into the mean for estimation:

$$\begin{aligned} p_\theta(\mathbf{x}_{t-1} | \mathbf{x}_t, y) &= \mathcal{N}(\boldsymbol{\mu}_\theta(\mathbf{x}_t, t, y), \sigma_t^2 \mathbf{I}) \\ &= \mathcal{N}\left(\sqrt{\frac{\bar{\alpha}_{t-1}}{\bar{\alpha}_t}}\mathbf{x}_t + \left(\sqrt{1 - \bar{\alpha}_{t-1} - \sigma_t^2} - \sqrt{\frac{\bar{\alpha}_{t-1}(1 - \bar{\alpha}_t)}{\bar{\alpha}_t}}\right)\boldsymbol{\epsilon}_\theta(\mathbf{x}_t, t, y), \sigma_t^2 \mathbf{I}\right), \end{aligned} \quad (6)$$

and the training loss function is:

$$\mathcal{L} \propto \mathbb{E}_{t, \mathbf{x}_t, \boldsymbol{\epsilon}_t} [\|\boldsymbol{\epsilon}_t - \boldsymbol{\epsilon}_\theta(\mathbf{x}_t, t, y)\|^2]. \quad (7)$$

The noise model $\boldsymbol{\epsilon}_\theta(\mathbf{x}_t, t, y)$ incorporates conditioning on y , guiding the denoising process towards the conditioned direction, thereby enabling conditional sampling and generation.

3 AMDM

In this section, we first analyze the challenges and limitations of current fine-grained control research, and establish the existence and applicability of aggregation algorithms. We then describe the design principles and propose the final algorithm, AMDM.

3.1 Analysis

Current fine-grained conditional control models tend to have limited control capabilities and face numerous issues. For example, given the caption "A red hair girl is drinking from a blue bottle of water, oil painting" and corresponding bounding boxes for positioning control, different models are likely to show varying performance, as illustrated in Figure 1. Model A, which receives additional inputs for position information and actions, excels in generating high-quality generation of positioning and interactions. However, it struggles with attribute control and maintaining the oil painting style. Conversely, Model B incorporates extra input for position and attribute information, managing both but not accurately capturing interactions and stylistic elements. Model C references the style of an image, enabling precise management of style characteristics but lacking adequate control over location and attribute details.

The fundamental reason for these issues lies in the complexity and flexibility of fine-grained control tasks, which makes it challenging for limited datasets and specific model architectures to account for all the intricate features. Although implementing a specific feature for a particular task is relatively straightforward, integrating these features for fine-grained control remains a significant challenge.

While different models may have varying additional input conditions, these conditions are often mutually compatible, leading to consistent objectives, which allows the models to generate similar images within their respective generation domains. Theoretically, model A has the capability to generate images that meet all the composite conditions of the caption for fine-grained control, although a single sampling might not fully activate this capability. It is noteworthy that these models share a common theoretical foundation, as they are all predicated on the same diffusion process and Classifier-Free Guidance (CFG) conditional control mechanism. Recognizing this shared basis, our

Caption: A red hair girl is drinking a blue bottle of water, oil painting



Figure 1: Examples of fine-grained conditional control of the same caption by different models.

objective is to develop an aggregation algorithm that leverages these commonalities to integrate the distinctive characteristics of multiple models into a specific model, achieving fine-grained conditional control in a more direct and efficient manner.

Do aggregation operations exist in different diffusion models? For a diffusion model p_θ , we define its generation domain at t under condition y as $D_{t,y}^\theta = \{\mathbf{x}_t \in \mathbb{R}^n \mid \mathbf{x}_t \sim p_\theta(\mathbf{x}_t|y)\}$. The generation domain $D_{t,y}^\theta$ represents the set of all intermediate variables at t generated by model θ under the condition y . Clearly, $D_{t,y}^\theta \subset \mathcal{M}_t$, where $\mathcal{M}_t = \{\mathbf{x}_t \in \mathbb{R}^n, \mathbf{x}_t \sim p(\mathbf{x}_t)\}$ which is independent of θ . Further, ensuring the consistency of \mathcal{M}_t guarantees the closure of intermediate variable operations across different $D_{t,y}^\theta$. This requires the same diffusion process to ensure consistency in the marginal distribution $p(\mathbf{x}_t)$ across models, as well as alignment of latent space encoders, if they exist. Therefore, operations within the generation domains of different models that share the same diffusion process at time t can remain closed within \mathcal{M}_t , which indicates that the aggregation algorithm is exist under such conditions.

Which models can achieve fine-grained generation through aggregation operations? Given a set of different diffusion models $M = \{p_{\theta_1}, p_{\theta_2}, \dots, p_{\theta_N}\}$, and corresponding conditions $Y = \{y_1, y_2, \dots, y_N\}$, if $\bigcap_{i=1}^N D_{t,y_i}^{\theta_i} \neq \emptyset$, then we define M as the t -compatible model set under condition Y . This indicates that there exists an intersection on the manifold where \mathbf{x}_t resides under different conditions corresponding to various diffusion models within M . Evidently, the points at these intersections encapsulate all the information of the condition Y . Therefore, intermediate variables \mathbf{x}_t of any model encapsulate all conditional information, enabling the generation of images under additional composite conditions. For a specific fine-grained control task, although different models may accept varying additional input types, they share a common objective. If this task is decomposed into different conditions y_1, y_2, \dots, y_N recognizable by different models, there must exist intermediate variables \mathbf{x}_t that satisfy each of these conditions for any $t \in [0, T]$. Consequently, these models collectively form a t -compatible model set under the task condition $Y = \{y_1, y_2, \dots, y_n\}$. This suggests that, in practical applications, almost all models can form a t -compatible model set under a specific task condition Y , enabling generation under composite conditions and achieving fine-grained control, providing a foundation for the design of the subsequent algorithm.

3.2 Algorithm

Based on the above analysis, our goal is to identify an aggregation operation that is closed on the manifold. For simplicity, we begin by considering the case of two models, specifically focusing on aggregating the conditional control information from p_{θ_2} into p_{θ_1} .

Spherical Aggregation. Sampling \mathbf{x}_0 from the model p_{θ_1} involves a series of reverse diffusion steps: $p_{\theta_1}(\mathbf{x}_T) \sim N(\mathbf{0}, \mathbf{I})$, $p_{\theta_1}(\mathbf{x}_{T-1}^{\theta_1} | \mathbf{x}_T^{\theta_1}, y_1)$, \dots , $p_{\theta_1}(\mathbf{x}_0^{\theta_1} | \mathbf{x}_1^{\theta_1}, y_1)$, signifying that $\mathbf{x}_t^{\theta_1} \in D_{t,y_1}^{\theta_1}$ for all $t \in [0, T]$. It indicates that the new intermediate variable must also reside within $D_{t,y_i}^{\theta_1} \subset \mathcal{M}_t$ for the sampling of p_{θ_1} , after aggregating another model p_{θ_2} . To find the optimal aggregation strategy, we next consider the properties of \mathcal{M}_t .

In the data space, Chung[30] has proven that \mathcal{M}_t is concentrated on an $(n-1)$ -dimensional manifold, which approximates an n -dimensional hypersphere as t becomes large. Currently, most fine-grained models are based on latent space diffusion models, and we observe that the corresponding \mathcal{M}_t is always concentrated on an n -dimensional hypersphere for any t . The relevant proof can be found in Appendix B. This motivates the use of spherical linear interpolation as the aggregation strategy, which maximizes the retention of the aggregated data on the original manifold with minimal deviations:

$$\begin{aligned} \mathbf{x}'_{t-1} &= \text{Slerp}(\mathbf{x}_{t-1}^{\theta_1}, \mathbf{x}_{t-1}^{\theta_2}, w) \\ &= \frac{\sin((1-w)\theta)}{\sin(\theta)} \mathbf{x}_{t-1}^{\theta_1} + \frac{\sin(w\theta)}{\sin(\theta)} \mathbf{x}_{t-1}^{\theta_2}, \\ \theta &= \cos^{-1}(\mathbf{x}_{t-1}^{\theta_1} \cdot \mathbf{x}_{t-1}^{\theta_2}) \end{aligned} \quad (8)$$

where \mathbf{x}'_{t-1} represents the aggregated intermediate variable, $\mathbf{x}_{t-1}^{\theta_1}$ and $\mathbf{x}_{t-1}^{\theta_2}$ are sampled from $p_{\theta_1}(\mathbf{x}_{t-1}^{\theta_1} | \mathbf{x}_t^{\theta_1}, y_1)$ and $p_{\theta_2}(\mathbf{x}_{t-1}^{\theta_2} | \mathbf{x}_t^{\theta_2}, y_2)$ respectively, and $w \in [0, 1]$ is the weighting factor that

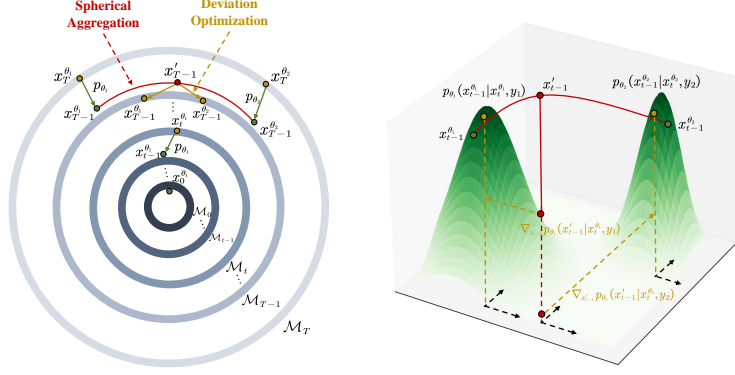


Figure 2: Geometry of AMDM (Left) and Deviation Optimization (Right). The algorithm employs spherical aggregation and deviation optimization to incorporate conditional information during the initial steps. Subsequently, direct sampling is applied to expedite the process and generate high-quality images.

balances the contribution of each model. Spherical aggregation integrates the conditional control information of p_{θ_2} into p_{θ_1} , while keeping the new variables stable near the manifold.

Deviation Optimization. Ideally, x'_{t-1} would reside on $D_{t-1,y_1}^{\theta_1} \cap D_{t-1,y_2}^{\theta_2}$, but deviations are likely to occur in practice. Considering the step from t to $t-1$, since $p_{\theta_1}(\mathbf{x}_{t-1}^{\theta_1} | \mathbf{x}_t^{\theta_1}, y_1)$ follows a normal distribution, a single sample is to be drawn with high confidence, which suggests that $D_{t,y_1}^{\theta_1}$ is consistently concentrated near the mean. As a result, we can shift x'_{t-1} along the gradient of the probability density function $p_{\theta_1}(\mathbf{x}_{t-1}^{\theta_1} | \mathbf{x}_t^{\theta_1}, y_1)$ by performing gradient ascent, adjusting the value to position it near the mean and bringing it back to $D_{t-1,y_1}^{\theta_1}$. In light of this, we propose the main proposition of the deviation optimization:

Proposition 3.1. For the diffusion model p_{θ_1} and any new intermediate variable \mathbf{x}'_{t-1} , let:

$$\mathbf{x}_{t-1}^{\theta_1} = \mathbf{x}'_{t-1} - \eta_{t-1}^{\theta_1} \frac{\mathbf{x}'_{t-1} - \mu_{\theta_1}(\mathbf{x}_t^{\theta_1}, t, y_1)}{\|\mathbf{x}'_{t-1} - \mu_{\theta_1}(\mathbf{x}_t^{\theta_1}, t, y_1)\|}, \quad (9)$$

then, $\mathbf{x}_{t-1}^{\theta_1}$ is corrected onto $D_{t-1,y_1}^{\theta_1}$. Here, $\mu_{\theta_1}(\mathbf{x}_t^{\theta_1}, t, y_1)$ is defined by (6), $\eta_{t-1}^{\theta_1}$ is a small optimization step size.

Proof is provided in Appendix A, and the geometry of deviation optimization is illustrated in Figure 2 (Right). Proposition 3.1 demonstrates that the intermediate variable can be corrected in a straightforward way to reside on $D_{t-1,y_1}^{\theta_1}$, thereby improving sampling quality. Furthermore, since the new variable contains information from p_{θ_2} , we can infer that it indeed resides on $D_{t-1,y_1}^{\theta_1} \cap D_{t-1,y_2}^{\theta_2}$, thus fulfilling the expectation of aggregation. We also introduce an adjustable aggregation step s , allowing flexible control over whether to incorporate information from other models.

Combining equations (8) and (9), the algorithm for aggregation of two diffusion models is presented, comprising two key components: spherical aggregation and deviation optimization. Spherical aggregation aggregates the conditional control information from different models and ensures that the new intermediate variables remain stable near the manifold, while deviation optimization ensures more precise retention on the corresponding data manifold, enhancing sample quality. The algorithm iteratively performs spherical aggregation and deviation optimization for each model during the first s steps, followed by direct sampling from p_{θ_1} . Note that each step of spherical aggregation also necessitates deviation optimization for p_{θ_2} to preserve the relevant conditional information within it, facilitating the subsequent aggregation step, as shown in Figure 2 (Left). This algorithm can be readily extended to multiple models, leading to the final Aggregation of Multi Diffusion Models (AMDM) algorithm, as shown in Algorithm 1. Moreover, since $\mu_{\theta_i}(\mathbf{x}_t^{\theta_i}, t, y_i)$ can reuse $\epsilon_{\theta_i}(\mathbf{x}_t^{\theta_i}, t, y_i)$ from the previous sampling step, the deviation optimization only introduces a single mathematical operation with no additional computational overhead, avoiding extra inference time.

Algorithm 1 AMDM

Input: t -compatible model set $M = \{p_{\theta_1}, p_{\theta_2}, \dots, p_{\theta_N}\}$ under condition $Y = \{y_1, y_2, \dots, y_N\}$, aggregation step s , weighting factor w_1, w_2, \dots, w_{N-1} and optimization step $\eta_t^{\theta_1}, \eta_t^{\theta_2}, \dots, \eta_t^{\theta_N}$
 $\mathbf{x}_T^{\theta_1}, \mathbf{x}_T^{\theta_2}, \dots, \mathbf{x}_T^{\theta_N} \sim N(\mathbf{0}, \mathbf{I})$
for t in $[T : 1]$ **do**
 $\mathbf{x}_{t-1}^{\theta_1} \sim p_{\theta_1}(\mathbf{x}_{t-1}^{\theta_1} | \mathbf{x}_t^{\theta_1}, y_1)$
if $t > T - s$ **then**
 $\mathbf{x}_{t-1}^{\theta_i} \sim p_{\theta_i}(\mathbf{x}_{t-1}^{\theta_i} | \mathbf{x}_t^{\theta_i}, y_i), i \in [2, N]$
 $\mathbf{x}'_{t-1} = \text{Slerp}(\mathbf{x}_{t-1}^{\theta_1}, \dots, \mathbf{x}_{t-1}^{\theta_N}, w_1, \dots, w_{N-1})$
 $\mathbf{x}_{t-1}^{\theta_i} = \mathbf{x}'_{t-1} - \eta_t^{\theta_i} \frac{\mathbf{x}'_{t-1} - \mu_{\theta}(\mathbf{x}_t^{\theta_i}, t, y_i)}{\|\mathbf{x}'_{t-1} - \mu_{\theta}(\mathbf{x}_t^{\theta_i}, t, y_i)\|}, i \in [1, N]$
end if
end for
Output: $x_0^{\theta_1}$

4 Experiments

In this section, we aggregate the classic conditional diffusion models and followed by a series of ablation experiments to demonstrate its optimality. The core idea of our experiment to demonstrate the effectiveness of the AMDM algorithm is as follows: Given a set of baseline models with varying control capabilities, we only need to focus on whether the target model, after aggregating features from other models, can enhance its performance in areas of weak control, reaching the level of the stronger models, while simultaneously preserving its own control advantages. All experiments were conducted using a single RTX 3090 GPU.

4.1 InteractDiffusion and MIGC

InteractDiffusion [17] is a T2I model that combines a pretrained Stable Diffusion (SD) model with a locally controlled interaction mechanism, enabling fine-grained control over the generated images and demonstrating effective interactivity. Similarly, MIGC [26] is a T2I model that employs a divide-and-conquer strategy, achieving excellent performance in both attribute representation and isolation of generated instances.

Table 1: Quantitative results on the HOI Detection Score, FID and CLIP Score across different models.

Method	Default \uparrow		Known Object \uparrow		FID \downarrow	CLIP Score \uparrow
	Full	Rare	Full	Rare		
MIGC	16.87	18.05	17.84	19.02	30.53	27.36
MIGC(+InteractDiffusion)	26.04	21.73	27.02	22.89	22.32	27.55
InteractDiffusion	29.53	23.02	30.99	24.93	18.69	26.91
InteractDiffusion(+MIGC)	31.40	24.52	32.76	26.32	18.35	27.18

InteractDiffusion primarily focuses on controlling subject-object interactions. However, due to the lack of explicit constraints on object attributes within the model architecture and dataset design, it exhibits suboptimal performance in attribute control. To address this, we attempt to aggregate the features of MIGC p_{θ_2} into InteractDiffusion p_{θ_1} by applying the AMDM algorithm, introducing attribute control information, and denoting this as InteractDiffusion(+MIGC). The total sampling steps T are set to 50, the aggregation step s is set to 20, the weighting factor w is set to 0.5 and the optimization steps $\eta_t^{\theta_1}$ and $\eta_t^{\theta_2}$ are both set to 0.3. We use InteractDiffusion v1.0, and MIGC is modified to use the DDIM sampling method to align with the same diffusion process. Experimental results are shown in Figure 3a. It is evident that aggregating the MIGC model into InteractDiffusion using our proposed AMDM algorithm significantly enhances its learned representations, leading to a notable improvement in instance attribute control, and confirming the algorithm’s effectiveness.

MIGC demonstrates strong attribute control on the COCO-MIG benchmark [26], while InteractDiffusion mainly uses the FGAHOI [31] for Human-Object Interaction (HOI) detection to show its control over interaction. To further validate the effectiveness of AMDM, we evaluate whether MIGC(+InteractDiffusion) can retain attribute control on COCO-MIG while significantly enhancing HOI interaction—ideally reaching the performance level of InteractDiffusion. Conversely, we also examine whether InteractDiffusion(+MIGC) can preserve interaction control while improving attribute control to match that of MIGC. Next, we provide a detailed introduction to the COCO-MIG benchmark and FGAHOI, along with the associated experimental setup.

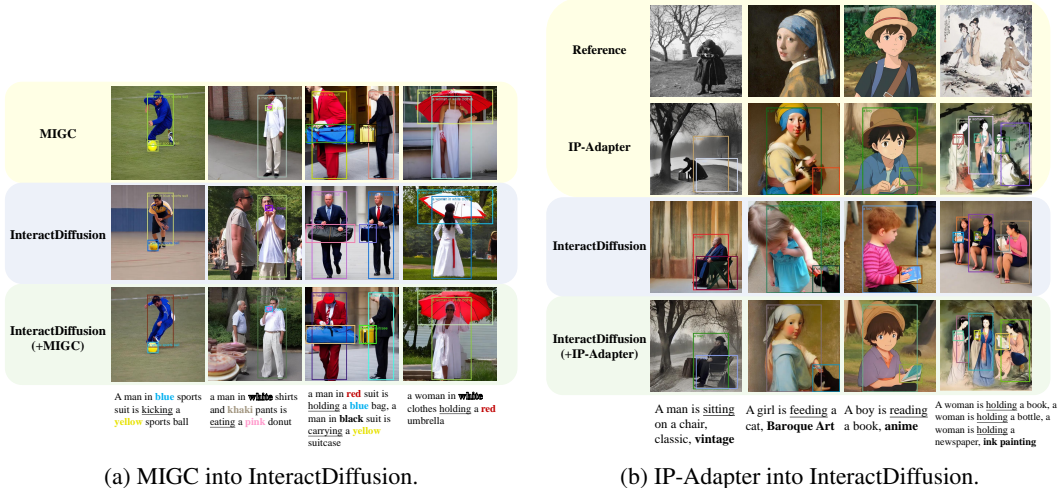


Figure 3: Visual results of applying AMDM algorithm.

Table 2: Quantitative results on the COCO-MIG benchmark and CLIP Score across different models.

Method	Instance Success Rate (%) \uparrow						mIoU Score (%) \uparrow						CLIP Score \uparrow	
	L_2	L_3	L_4	L_5	L_6	Avg	L_2	L_3	L_4	L_5	L_6	Avg	Global	Local
InteractDiffusion	37.50	35.62	35.31	30.62	34.16	34.06	32.98	31.63	30.82	28.29	30.40	30.40	31.09	27.56
InteractDiffusion(+MIGC)	62.29	54.33	56.31	53.87	52.89	54.78	54.30	46.37	48.44	47.65	46.64	47.74	32.81	28.96
MIGC	64.06	56.04	58.43	56.00	49.89	55.46	54.43	49.33	50.48	48.67	44.74	48.53	32.78	28.61
MIGC(+InteractDiffusion)	60.00	50.20	50.46	48.25	46.97	49.78	52.58	44.27	43.39	42.67	41.50	43.69	32.41	28.55

COCO-MIG Benchmark [26] assess the enhancement in attribute metrics. The COCO-MIG Benchmark is based on the COCO-position layout, where each instance is assigned a color attribute, requiring the generated instances to satisfy both position and color constraints. The process includes sampling layouts from COCO and categorizing layouts into five levels (L_2 - L_6) based on the number of instances. Then, colors are assigned to each instance, global prompts are constructed, and a test file containing 800 entries is generated. The COCO-MIG metrics primarily include Instance Success Rate and mIoU Score. The Instance Success Rate measures the probability of each instance being generated correctly, while mIoU Score calculates the average of the maximum IoU for all instances; if the color attribute is incorrect, the IoU value is set to 0. Since the MIG-Benchmark does not contain interactive prompt, we set the "action" input in the InteractDiffusion model to "and".

FGAHOI [31] can measure interaction controllability. We use the FGAHOI model based on the Swin-Tiny architecture, as an HOI detector to evaluate the model's ability to control interactions. HOI Detection Scores are categorized into two types: Default and Known Object. The Default setting is more challenging, as it requires distinguishing between irrelevant images.

The quantitative results of InteractDiffusion(+MIGC) are shown in the first two rows of Table 2. It can be observed that all metrics have significantly improved in InteractDiffusion(+MIGC) in attribute control. Interestingly, as shown in the last two rows of Table 1, it even surpasses the original InteractDiffusion model in terms of interaction. Similarly, the results of MIGC(+InteractDiffusion) are shown in the first two rows of Table 1. It can be seen that MIGC(+InteractDiffusion) also shows significant improvements across all metrics in the interaction capability control. Additionally, as observed in the last two rows of Table 2, the MIGC(+InteractDiffusion) maintains the original performance of MIGC in attribute control, validating the effectiveness of the algorithm.

4.2 InteractDiffusion and IP-Adapter

IP-Adapter [28] is a lightweight I2I model that employs a decoupled cross-attention mechanism to separately process text and image features, enabling multimodal image generation. Due to its superior performance in preserving the style of the reference image, we propose integrating the style information from IP-Adapter p_{θ_3} into InteractDiffusion p_{θ_1} , denoted as InteractDiffusion(+IP-Adapter). The total sampling steps T are set to 10, the aggregation step s is set to 5, the weighting

factor w is set to 0.5, ip scale is set to 0.8 and the optimization steps $\eta_t^{\theta_1}$ and $\eta_t^{\theta_3}$ are both set to 0.3. We utilized IP-Adapter based on SD1.5 while keeping InteractDiffusion unchanged. The experimental results are shown in Figure 3b. It can be observed that IP-Adapter enhances the style representations of InteractDiffusion, fully activating its style controllability, which further validates the effectiveness of the algorithm.

4.3 InteractDiffusion, MIGC and IP-Adapter

Furthermore, we attempt to aggregate the attribute features from MIGC p_{θ_2} and the style features from IP-Adapter p_{θ_3} into InteractDiffusion p_{θ_1} to evaluate the effectiveness of the AMDM algorithm. The pretrained models for the three architectures remain consistent with those mentioned above. The total sampling step T set to 10, an aggregation step s set to 5, and weight factors w_1 and w_2 set to 0.5 and 0.65. The optimization steps $\eta_t^{\theta_1}$, $\eta_t^{\theta_2}$, and $\eta_t^{\theta_3}$ are all simply set to 0.3, respectively. The experimental results are presented in Figure 4.

Furthermore, the fact that fine-grained generation can be achieved by aggregating only the first s steps indicates that diffusion models initially focus on features such as position, attributes, and style, while the later stages emphasize generation quality and consistency. Vice versa, this allows aggregation algorithms to be used only in the first s steps, significantly reducing computational overhead.



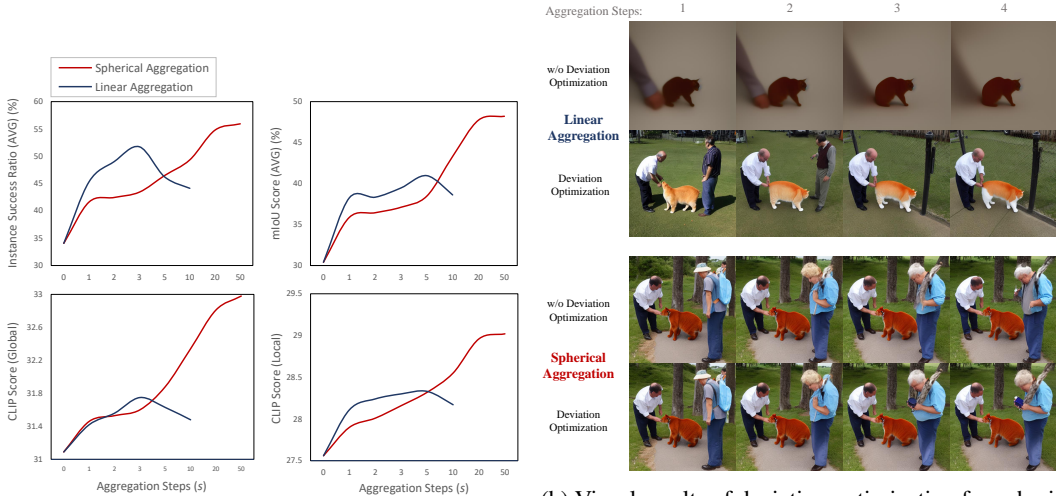
Figure 4: Visual results of aggregating MIGC and IP-Adapter into InteractDiffusion.

4.4 Ablation Studies

The AMDM algorithm consists of two key components: spherical aggregation and deviation optimization, with the aggregation degree controlled by the number of aggregation steps s . Therefore, in this section, we primarily conduct ablation studies on these aspects in the aggregation experiments of InteractDiffusion(+MIGC).

We attempt a comparison with linear aggregation which has been of broad interest in compositional generation and the results are shown in the Figure 5a. It can be observed that when the number of aggregation steps is small ($s < 5$), linear aggregation performs slightly better than spherical aggregation. However, as the number of aggregation steps increases, spherical aggregation significantly outperforms linear aggregation across various metrics. This is because, with more aggregation steps, the cumulative error due to the deviation in the data manifold becomes increasingly larger in linear aggregation, which negatively impacts the image quality. As shown in Figure 5b, the characteristic of manifold deviation in linear aggregation is evident. In contrast, spherical aggregation consistently minimizes the deviation of the aggregated variables from the spherical manifold, preserving the quality of the final image as much as possible. The deviation optimization further enhances the image quality, demonstrating its effectiveness. Considering both performance and efficiency, spherical aggregation reaches optimum at 20 steps in this experiment. A more detailed discussion of compositional methods can be found in the Related Work and Appendix C.

We also investigated the optimization step of deviation optimization, with experimental results shown in the Table 3. Obviously, when the optimization step is set to 0.3, the best performance is achieved across all metrics. Moreover, the results outperform those achieved with 50 aggregation steps without optimization.



(a) Metrics of spherical aggregation and linear aggregation under different aggregation steps.

(b) Visual results of deviation optimization for spherical aggregation and linear aggregation under different aggregation steps.

Figure 5: Ablation study.

Table 3: Ablation results of different deviation optimization step on COCO-MIG benchmark in InteractDiffusion(+MIGC).

Deviation Optimization Step	Instance Success Rate (%) ↑						mIoU Score (%) ↑						CLIP Score ↑	
	L_2	L_3	L_4	L_5	L_6	Avg	L_2	L_3	L_4	L_5	L_6	Avg	Global	Local
0	61.56	52.08	53.75	51.62	51.87	53.18	54.76	45.09	46.36	45.48	45.79	46.62	31.09	27.56
0.1	57.60	53.26	53.89	52.40	52.08	53.26	53.27	45.53	46.86	46.31	45.80	46.83	31.43	27.87
0.2	59.62	54.27	54.06	51.25	52.29	53.40	52.71	46.32	47.17	44.68	45.74	46.59	31.92	28.45
0.3	62.29	54.33	56.31	53.87	52.89	54.78	54.30	46.37	48.44	47.65	46.64	47.74	32.81	28.96
0.4	61.34	53.62	55.32	52.22	52.50	53.96	53.46	46.21	46.82	45.26	46.23	46.78	32.23	28.55
0.5	58.30	53.43	55.14	51.76	51.76	53.27	52.88	45.03	46.52	44.95	45.51	46.14	31.15	27.78

5 Related Works

Fine-Grained Generation. In addition to text-driven models [9, 32, 6, 33, 34], an increasing number of studies are exploring more advanced and finer-grained conditional control techniques. One of the most classical approaches is personalization controlled generation, including style generation [35, 36, 37, 38], subject-driven generation [39, 40, 41, 42, 28], person-driven generation [43, 44, 45, 46, 47], and interactive generation [48, 49, 50, 17]. Additionally, spatial-controlled generation [25, 51, 52, 53, 26] represents another significant research focus, primarily leveraging bounding boxes or various regions as additional input conditions to achieve specific spatial control objectives. In recent years, several studies have attempted to directly achieve fine-grained control [54, 55, 56, 57, 58] by designing various model architectures to handle inputs from various modalities, which require extensive training. These approaches inevitably necessitate a substantial amount of comprehensive multi-condition fine-grained data and the development of complex model architectures.

Compositional Generation. Some recent work [59, 60, 61, 62, 63, 64, 65, 66] aim to create new distributions by combining two different distributions, commonly using techniques such as linear weighted score, followed by simulated annealing or other optimization methods. In contrast, AMDM focuses on fine-grained generation, where the input remains consistent. In fact, this paper is the first to propose a training-free aggregation method for fine-grained generation tasks, seeking to find the intersection of two Gaussian distributions that satisfies all conditions, without generating a new distribution, but rather strengthening consistency for the same object. A more in-depth comparison of our AMDM and its relation to compositional generation methods can be found in the Appendix C.

6 Conclusion

This paper proposes a novel AMDM algorithm designed for fine-grained generation, which consists of two main components: spherical aggregation and deviation optimization. Experimental results

demonstrate the effectiveness of the AMDM algorithm, revealing that diffusion models initially prioritize image feature generation, shifting their focus to image quality and consistency in later stages. The algorithm provides a new perspective for addressing fine-grained generation challenge: We can leverage existing or develop new conditional diffusion models that control specific aspects, and then aggregate them using the AMDM algorithm. This eliminates the need for constructing complex datasets, designing intricate model architectures, and incurring high training costs.

References

- [1] J. Sohl-Dickstein, E. Weiss, N. Maheswaranathan, and S. Ganguli, “Deep unsupervised learning using nonequilibrium thermodynamics,” in *International conference on machine learning*. PMLR, 2015, pp. 2256–2265.
- [2] J. Ho, A. Jain, and P. Abbeel, “Denoising diffusion probabilistic models,” *Advances in neural information processing systems*, vol. 33, pp. 6840–6851, 2020.
- [3] J. Song, C. Meng, and S. Ermon, “Denoising diffusion implicit models,” in *International Conference on Learning Representations*, 2021.
- [4] Y. Song, J. Sohl-Dickstein, D. P. Kingma, A. Kumar, S. Ermon, and B. Poole, “Score-based generative modeling through stochastic differential equations,” in *Proceedings of International Conference on Learning Representations (ICLR)*, 2021.
- [5] T. Karras, M. Aittala, T. Aila, and S. Laine, “Elucidating the design space of diffusion-based generative models,” *Advances in Neural Information Processing Systems*, vol. 35, pp. 26 565–26 577, 2022.
- [6] R. Rombach, A. Blattmann, D. Lorenz, P. Esser, and B. Ommer, “High-resolution image synthesis with latent diffusion models,” in *Proceedings of the IEEE/CVF conference on computer vision and pattern recognition*, 2022, pp. 10 684–10 695.
- [7] H. Chung, J. Kim, M. T. Mccann, M. L. Klasky, and J. C. Ye, “Diffusion posterior sampling for general noisy inverse problems,” in *The Eleventh International Conference on Learning Representations*, 2023.
- [8] P. Esser, S. Kulal, A. Blattmann, R. Entezari, J. Müller, H. Saini, Y. Levi, D. Lorenz, A. Sauer, F. Boesel *et al.*, “Scaling rectified flow transformers for high-resolution image synthesis,” in *Forty-first International Conference on Machine Learning*, 2024.
- [9] A. Q. Nichol, P. Dhariwal, A. Ramesh, P. Shyam, P. Mishkin, B. McGrew, I. Sutskever, and M. Chen, “Glide: Towards photorealistic image generation and editing with text-guided diffusion models,” in *International Conference on Machine Learning*. PMLR, 2022, pp. 16 784–16 804.
- [10] W. Chen, H. Hu, C. Saharia, and W. W. Cohen, “Re-imagen: Retrieval-augmented text-to-image generator,” in *The Eleventh International Conference on Learning Representations*, 2023.
- [11] T. Lee, M. Yasunaga, C. Meng, Y. Mai, J. S. Park, A. Gupta, Y. Zhang, D. Narayanan, H. Teufel, M. Bellagente *et al.*, “Holistic evaluation of text-to-image models,” *Advances in Neural Information Processing Systems*, vol. 36, 2024.
- [12] J. Xu, X. Liu, Y. Wu, Y. Tong, Q. Li, M. Ding, J. Tang, and Y. Dong, “Imagereward: Learning and evaluating human preferences for text-to-image generation,” *Advances in Neural Information Processing Systems*, vol. 36, 2024.
- [13] Y. Zhang, N. Huang, F. Tang, H. Huang, C. Ma, W. Dong, and C. Xu, “Inversion-based style transfer with diffusion models,” in *Proceedings of the IEEE/CVF conference on computer vision and pattern recognition*, 2023, pp. 10 146–10 156.
- [14] C. Mou, X. Wang, J. Song, Y. Shan, and J. Zhang, “Diffeditor: Boosting accuracy and flexibility on diffusion-based image editing,” in *Proceedings of the IEEE/CVF Conference on Computer Vision and Pattern Recognition*, 2024, pp. 8488–8497.
- [15] Q. Wu, Y. Liu, H. Zhao, A. Kale, T. Bui, T. Yu, Z. Lin, Y. Zhang, and S. Chang, “Uncovering the disentanglement capability in text-to-image diffusion models,” in *Proceedings of the IEEE/CVF conference on computer vision and pattern recognition*, 2023, pp. 1900–1910.
- [16] R. Wang, Z. Chen, C. Chen, J. Ma, H. Lu, and X. Lin, “Compositional text-to-image synthesis with attention map control of diffusion models,” in *Proceedings of the AAAI Conference on Artificial Intelligence*, vol. 38, 2024, pp. 5544–5552.

- [17] J. T. Hoe, X. Jiang, C. S. Chan, Y.-P. Tan, and W. Hu, “Interactdiffusion: Interaction control in text-to-image diffusion models,” in *Proceedings of the IEEE/CVF Conference on Computer Vision and Pattern Recognition*, 2024, pp. 6180–6189.
- [18] X. Jia, T. Isobe, X. Li, Q. Wang, J. Mu, D. Zhou, H. Lu, L. Tian, A. Sirasao, E. Barsoum *et al.*, “Customizing text-to-image generation with inverted interaction,” in *ACM Multimedia 2024*, 2024.
- [19] G. Zheng, X. Zhou, X. Li, Z. Qi, Y. Shan, and X. Li, “Layoutdiffusion: Controllable diffusion model for layout-to-image generation,” in *Proceedings of the IEEE/CVF Conference on Computer Vision and Pattern Recognition*, 2023, pp. 22 490–22 499.
- [20] S. Chai, L. Zhuang, and F. Yan, “Layoutdm: Transformer-based diffusion model for layout generation,” in *Proceedings of the IEEE/CVF Conference on Computer Vision and Pattern Recognition*, 2023, pp. 18 349–18 358.
- [21] J. Chen, Y. Huang, T. Lv, L. Cui, Q. Chen, and F. Wei, “Textdiffuser: Diffusion models as text painters,” *Advances in Neural Information Processing Systems*, vol. 36, 2024.
- [22] Z. Wang, L. Zhao, and W. Xing, “Stylediffusion: Controllable disentangled style transfer via diffusion models,” in *Proceedings of the IEEE/CVF International Conference on Computer Vision*, 2023, pp. 7677–7689.
- [23] N. Huang, Y. Zhang, F. Tang, C. Ma, H. Huang, W. Dong, and C. Xu, “Diffstyler: Controllable dual diffusion for text-driven image stylization,” *IEEE Transactions on Neural Networks and Learning Systems*, 2024.
- [24] T. Qi, S. Fang, Y. Wu, H. Xie, J. Liu, L. Chen, Q. He, and Y. Zhang, “Deadiff: An efficient stylization diffusion model with disentangled representations,” in *Proceedings of the IEEE/CVF Conference on Computer Vision and Pattern Recognition*, 2024, pp. 8693–8702.
- [25] Y. Li, H. Liu, Q. Wu, F. Mu, J. Yang, J. Gao, C. Li, and Y. J. Lee, “Gligen: Open-set grounded text-to-image generation,” in *Proceedings of the IEEE/CVF Conference on Computer Vision and Pattern Recognition*, 2023, pp. 22 511–22 521.
- [26] D. Zhou, Y. Li, F. Ma, X. Zhang, and Y. Yang, “Migc: Multi-instance generation controller for text-to-image synthesis,” in *Proceedings of the IEEE/CVF Conference on Computer Vision and Pattern Recognition*, 2024, pp. 6818–6828.
- [27] X. Wang, T. Darrell, S. S. Rambhatla, R. Girdhar, and I. Misra, “Instancediffusion: Instance-level control for image generation,” in *Proceedings of the IEEE/CVF Conference on Computer Vision and Pattern Recognition*, 2024, pp. 6232–6242.
- [28] H. Ye, J. Zhang, S. Liu, X. Han, and W. Yang, “Ip-adapter: Text compatible image prompt adapter for text-to-image diffusion models,” *arXiv preprint arXiv:2308.06721*, 2023.
- [29] P. Dhariwal and A. Nichol, “Diffusion models beat gans on image synthesis,” *Advances in neural information processing systems*, vol. 34, pp. 8780–8794, 2021.
- [30] H. Chung, B. Sim, D. Ryu, and J. C. Ye, “Improving diffusion models for inverse problems using manifold constraints,” in *Advances in Neural Information Processing Systems*, 2022.
- [31] S. Ma, Y. Wang, S. Wang, and Y. Wei, “Fgahoi: Fine-grained anchors for human-object interaction detection,” *IEEE Transactions on Pattern Analysis and Machine Intelligence*, 2023.
- [32] A. Ramesh, P. Dhariwal, A. Nichol, C. Chu, and M. Chen, “Hierarchical text-conditional image generation with clip latents,” *arXiv preprint arXiv:2204.06125*, vol. 1, no. 2, p. 3, 2022.
- [33] H. Li, H. Shi, W. Zhang, W. Wu, Y. Liao, L. Wang, L.-h. Lee, and P. Zhou, “Dreamscene: 3d gaussian-based text-to-3d scene generation via formation pattern sampling,” *arXiv preprint arXiv:2404.03575*, 2024.
- [34] D. Podell, Z. English, K. Lacey, A. Blattmann, T. Dockhorn, J. Müller, J. Penna, and R. Rombach, “Sdxl: Improving latent diffusion models for high-resolution image synthesis,” in *The Twelfth International Conference on Learning Representations*, 2024.
- [35] K. Sohn, N. Ruiz, K. Lee, D. C. Chin, I. Blok, H. Chang, J. Barber, L. Jiang, G. Entis, Y. Li *et al.*, “Styler: text-to-image generation in any style,” in *Proceedings of the 37th International Conference on Neural Information Processing Systems*, 2023, pp. 66 860–66 889.

- [36] G. Liu, M. Xia, Y. Zhang, H. Chen, J. Xing, X. Wang, Y. Yang, and Y. Shan, “Stylecrafter: Enhancing stylized text-to-video generation with style adapter,” *arXiv preprint arXiv:2312.00330*, 2023.
- [37] A. Hertz, A. Voynov, S. Fruchter, and D. Cohen-Or, “Style aligned image generation via shared attention,” in *Proceedings of the IEEE/CVF Conference on Computer Vision and Pattern Recognition*, 2024, pp. 4775–4785.
- [38] D.-Y. Chen, H. Tennent, and C.-W. Hsu, “Artadapter: Text-to-image style transfer using multi-level style encoder and explicit adaptation,” in *Proceedings of the IEEE/CVF Conference on Computer Vision and Pattern Recognition*, 2024, pp. 8619–8628.
- [39] N. Ruiz, Y. Li, V. Jampani, Y. Pritch, M. Rubinstein, and K. Aberman, “Dreambooth: Fine tuning text-to-image diffusion models for subject-driven generation,” in *Proceedings of the IEEE/CVF conference on computer vision and pattern recognition*, 2023, pp. 22 500–22 510.
- [40] D. Li, J. Li, and S. Hoi, “Blip-diffusion: Pre-trained subject representation for controllable text-to-image generation and editing,” *Advances in Neural Information Processing Systems*, vol. 36, 2024.
- [41] J. Shi, W. Xiong, Z. Lin, and H. J. Jung, “Instantbooth: Personalized text-to-image generation without test-time finetuning,” in *Proceedings of the IEEE/CVF Conference on Computer Vision and Pattern Recognition*, 2024, pp. 8543–8552.
- [42] Y. Jiang, T. Wu, S. Yang, C. Si, D. Lin, Y. Qiao, C. C. Loy, and Z. Liu, “Videobooth: Diffusion-based video generation with image prompts,” in *Proceedings of the IEEE/CVF Conference on Computer Vision and Pattern Recognition*, 2024, pp. 6689–6700.
- [43] G. Xiao, T. Yin, W. T. Freeman, F. Durand, and S. Han, “Fastcomposer: Tuning-free multi-subject image generation with localized attention,” *International Journal of Computer Vision*, pp. 1–20, 2024.
- [44] N. Giambi and G. Lisanti, “Conditioning diffusion models via attributes and semantic masks for face generation,” *arXiv preprint arXiv:2306.00914*, 2023.
- [45] D. Valevski, D. Lumen, Y. Matias, and Y. Leviathan, “Face0: Instantaneously conditioning a text-to-image model on a face,” in *SIGGRAPH Asia 2023 Conference Papers*, 2023, pp. 1–10.
- [46] P. Achlioptas, A. Benetatos, I. Fostiropoulos, and D. Skourtis, “Stellar: Systematic evaluation of human-centric personalized text-to-image methods,” *arXiv preprint arXiv:2312.06116*, 2023.
- [47] X. Peng, J. Zhu, B. Jiang, Y. Tai, D. Luo, J. Zhang, W. Lin, T. Jin, C. Wang, and R. Ji, “Portraitbooth: A versatile portrait model for fast identity-preserved personalization,” in *Proceedings of the IEEE/CVF Conference on Computer Vision and Pattern Recognition*, 2024, pp. 27 080–27 090.
- [48] Z. Huang, T. Wu, Y. Jiang, K. C. Chan, and Z. Liu, “Reversion: Diffusion-based relation inversion from images,” *arXiv preprint arXiv:2303.13495*, 2023.
- [49] Y. Guo, C. Yang, A. Rao, Z. Liang, Y. Wang, Y. Qiao, M. Agrawala, D. Lin, and B. Dai, “Animatediff: Animate your personalized text-to-image diffusion models without specific tuning,” in *The Twelfth International Conference on Learning Representations*, 2024.
- [50] R. Wu, L. Chen, T. Yang, C. Guo, C. Li, and X. Zhang, “Lamp: Learn a motion pattern for few-shot-based video generation,” *arXiv preprint arXiv:2310.10769*, 2023.
- [51] J. Cheng, X. Liang, X. Shi, T. He, T. Xiao, and M. Li, “Layoutdiffuse: Adapting foundational diffusion models for layout-to-image generation,” *arXiv preprint arXiv:2302.08908*, 2023.
- [52] Y. Kim, J. Lee, J.-H. Kim, J.-W. Ha, and J.-Y. Zhu, “Dense text-to-image generation with attention modulation,” in *Proceedings of the IEEE/CVF International Conference on Computer Vision*, 2023, pp. 7701–7711.
- [53] W. Nie, S. Liu, M. Mardani, C. Liu, B. Eckart, and A. Vahdat, “Compositional text-to-image generation with dense blob representations,” in *Forty-first International Conference on Machine Learning*, 2024.
- [54] L. Huang, D. Chen, Y. Liu, Y. Shen, D. Zhao, and J. Zhou, “Composer: creative and controllable image synthesis with composable conditions,” in *Proceedings of the 40th International Conference on Machine Learning*, 2023, pp. 13 753–13 773.

- [55] L. Han, Y. Li, H. Zhang, P. Milanfar, D. Metaxas, and F. Yang, “Svdiff: Compact parameter space for diffusion fine-tuning,” in *Proceedings of the IEEE/CVF International Conference on Computer Vision*, 2023, pp. 7323–7334.
- [56] J. S. Smith, Y.-C. Hsu, L. Zhang, T. Hua, Z. Kira, Y. Shen, and H. Jin, “Continual diffusion: Continual customization of text-to-image diffusion with c-lora,” *arXiv preprint arXiv:2304.06027*, 2023.
- [57] Y. Gu, X. Wang, J. Z. Wu, Y. Shi, Y. Chen, Z. Fan, W. Xiao, R. Zhao, S. Chang, W. Wu *et al.*, “Mix-of-show: Decentralized low-rank adaptation for multi-concept customization of diffusion models,” *Advances in Neural Information Processing Systems*, vol. 36, 2024.
- [58] N. Kumari, B. Zhang, R. Zhang, E. Shechtman, and J.-Y. Zhu, “Multi-concept customization of text-to-image diffusion,” in *Proceedings of the IEEE/CVF Conference on Computer Vision and Pattern Recognition*, 2023, pp. 1931–1941.
- [59] Y. Du, S. Li, and I. Mordatch, “Compositional visual generation with energy based models,” *Advances in Neural Information Processing Systems*, vol. 33, pp. 6637–6647, 2020.
- [60] N. Liu, S. Li, Y. Du, A. Torralba, and J. B. Tenenbaum, “Compositional visual generation with composable diffusion models,” in *European Conference on Computer Vision*. Springer, 2022, pp. 423–439.
- [61] Y. Du, C. Durkan, R. Strudel, J. B. Tenenbaum, S. Dieleman, R. Fergus, J. Sohl-Dickstein, A. Doucet, and W. S. Grathwohl, “Reduce, reuse, recycle: Compositional generation with energy-based diffusion models and mcmc,” in *International conference on machine learning*. PMLR, 2023, pp. 8489–8510.
- [62] Y. Du and L. P. Kaelbling, “Position: Compositional generative modeling: A single model is not all you need,” in *Forty-first International Conference on Machine Learning*, 2024.
- [63] T. Garipov, S. De Peuter, G. Yang, V. Garg, S. Kaski, and T. Jaakkola, “Compositional sculpting of iterative generative processes,” *Advances in neural information processing systems*, vol. 36, pp. 12 665–12 702, 2023.
- [64] A. Bradley, P. Nakkiran, D. Berthelot, J. Thornton, and J. M. Susskind, “Mechanisms of projective composition of diffusion models,” *arXiv preprint arXiv:2502.04549*, 2025.
- [65] J. Thornton, L. Béthune, R. Zhang, A. Bradley, P. Nakkiran, and S. Zhai, “Composition and control with distilled energy diffusion models and sequential monte carlo,” *arXiv preprint arXiv:2502.12786*, 2025.
- [66] M. Skreta, T. Akhound-Sadegh, V. Ohanesian, R. Bondesan, A. Aspuru-Guzik, A. Doucet, R. Brekelmans, A. Tong, and K. Neklyudov, “Feynman-kac correctors in diffusion: Annealing, guidance, and product of experts,” *arXiv preprint arXiv:2503.02819*, 2025.
- [67] S. Särkkä and A. Solin, *Applied stochastic differential equations*. Cambridge University Press, 2019, vol. 10.

A Proof of Proposition 3.1

Proposition 3.1. For the diffusion model p_{θ_1} and any new intermediate variable \mathbf{x}'_{t-1} , let:

$$\mathbf{x}_{t-1}^{\theta_1} = \mathbf{x}'_{t-1} - \eta_{t-1}^{\theta_1} \frac{\mathbf{x}'_{t-1} - \mu_{\theta_1}(\mathbf{x}_t^{\theta_1}, t, y_1)}{\|\mathbf{x}'_{t-1} - \mu_{\theta_1}(\mathbf{x}_t^{\theta_1}, t, y_1)\|}, \quad (9)$$

then, $\mathbf{x}_{t-1}^{\theta_1}$ is corrected onto $D_{t-1, y_1}^{\theta_1}$. Here, $\mu_{\theta_1}(\mathbf{x}_t^{\theta_1}, t, y_1)$ is defined by (6), $\eta_{t-1}^{\theta_1}$ is a small optimization step size.

Proof: Our objective is to correct the new variable \mathbf{x}'_{t-1} , which deviates from $D_{t-1, y_1}^{\theta_1}$, to ensure proper generation in subsequent sampling. Considering the step from t to $t-1$, since $p_{\theta_1}(\mathbf{x}_{t-1}^{\theta_1} | \mathbf{x}_t^{\theta_1}, y_1)$ follows a normal distribution, the sampling process typically results in high-confidence clustering near the mean, causing the data to consistently reside in this region. Thus, we can move \mathbf{x}'_{t-1} along the gradient of the probability density function $p_{\theta_1}(\mathbf{x}'_{t-1} | \mathbf{x}_t^{\theta_1}, y_1)$ by performing gradient ascent, thereby adjusting the value toward the peak region and aligning the data with the manifold $\mathcal{M} = \{\mathbf{x}_{t-1}^{\theta_1} \sim p_{\theta_1}(\mathbf{x}_{t-1}^{\theta_1} | \mathbf{x}_t^{\theta_1}, y_1)\}$. Since \mathcal{M} is a submanifold of $D_{t-1, y_1}^{\theta_1}$, this optimization approach effectively pulls \mathbf{x}'_{t-1} back onto $D_{t-1, y_1}^{\theta_1}$. Therefore, our optimization objective is:

$$\arg \max_{\mathbf{x}'_{t-1} \in \bar{U}(\mathbf{x}'_{t-1}, \delta)} [\nabla_{\mathbf{x}'_{t-1}} p_{\theta_1}(\mathbf{x}'_{t-1} | \mathbf{x}_t^{\theta_1}, y_1)]^T (\mathbf{x}_{t-1}^{\theta_1} - \mathbf{x}'_{t-1}), \quad (10)$$

where $\bar{U}(\mathbf{x}'_{t-1}, \delta) = \{\mathbf{x} | \|\mathbf{x} - \mathbf{x}'_{t-1}\| \leq \delta\}$ and δ is a small adjusting step, then:

$$\begin{aligned} \mathbf{x}_{t-1}^{\theta_1} &= \mathbf{x}'_{t-1} + \delta \nabla_{\mathbf{x}'_{t-1}} p_{\theta_1}(\mathbf{x}'_{t-1} | \mathbf{x}_t^{\theta_1}, y_1) \\ &= \mathbf{x}'_{t-1} + \eta_{t-1}^{\theta_1} \frac{\nabla_{\mathbf{x}'_{t-1}} p_{\theta_1}(\mathbf{x}'_{t-1} | \mathbf{x}_t^{\theta_1}, y_1)}{\|\nabla_{\mathbf{x}'_{t-1}} p_{\theta_1}(\mathbf{x}'_{t-1} | \mathbf{x}_t^{\theta_1}, y_1)\|}, \end{aligned} \quad (11)$$

where $\eta_{t-1}^{\theta_1}$ is the step size for the unit gradient ascent. Since $p_{\theta_1}(\mathbf{x}'_{t-1} | \mathbf{x}_t^{\theta_1}, y_1)$ is a normal distribution, its gradient can be computed as follows:

$$\begin{aligned} \nabla_{\mathbf{x}'_{t-1}} p_{\theta_1}(\mathbf{x}'_{t-1} | \mathbf{x}_t^{\theta_1}, y_1) &= \frac{1}{(2\pi\sigma_t^2)^{n/2}} \nabla_{\mathbf{x}'_{t-1}} \left(e^{-\frac{\|\mathbf{x}'_{t-1} - \mu_{\theta_1}(\mathbf{x}_t^{\theta_1}, t, y_1)\|^2}{2\sigma_t^2}} \right) \\ &= -\frac{1}{(2\pi\sigma_t^2)^{n/2}} e^{-\frac{\|\mathbf{x}'_{t-1} - \mu_{\theta_1}(\mathbf{x}_t^{\theta_1}, t, y_1)\|^2}{2\sigma_t^2}} \left(\frac{\mathbf{x}'_{t-1} - \mu_{\theta_1}(\mathbf{x}_t^{\theta_1}, t, y_1)}{\sigma_t^2} \right). \end{aligned} \quad (12)$$

Simplifying the coefficient term, the final result is:

$$\mathbf{x}_{t-1}^{\theta_1} = \mathbf{x}'_{t-1} - \eta_{t-1}^{\theta_1} \frac{\mathbf{x}'_{t-1} - \mu_{\theta_1}(\mathbf{x}_t^{\theta_1}, t, y_1)}{\|\mathbf{x}'_{t-1} - \mu_{\theta_1}(\mathbf{x}_t^{\theta_1}, t, y_1)\|}, \quad (13)$$

which concludes the proof.

B Concentration of Latent Diffusion

In this section, we investigate the concentration of the marginal distribution for Stable Diffusion.

Lemma B.1. (Concentration of Measure Theorem for High-Dimensional Independent Normal Distribution). Let $X = (X_1, X_2, \dots, X_n)$ be an n -dimensional random vector where each component X_i is independently and identically distributed as $N(\mathbf{0}, \sigma^2 \mathbf{I})$. Then, as the dimension n increases, the norm $\|X\|$ of X is concentrated around $\sqrt{n}\sigma$. Specifically, for any small $\epsilon \geq 0$ and sufficiently large n ,

$$P(|\|X\| - \sqrt{n}\sigma| \leq \epsilon \sqrt{n}\sigma) \geq 1 - 2e^{-\frac{n\epsilon^2}{1+2\epsilon}} \quad (14)$$

This means X will concentrate near the hypersphere of radius $\sqrt{n}\sigma$ with high probability.

Proof: First, we consider the squared norm of a random vector X : $\|X\|^2 = X_1^2 + X_2^2 + \dots + X_n^2$. Since $X_i \sim \mathcal{N}(0, \sigma^2 \mathbf{I})$, it follows that $Y = \|X\|^2 / \sigma^2 \sim \chi^2(n)$.

Using the Chernoff bound of the chi-square distribution:

$$P(Y \geq (1 + \delta)n) \leq e^{-\frac{n}{2}[\delta - \ln(1 + \delta)]}, \quad (15)$$

$$P(Y \leq (1 - \delta)n) \leq e^{-\frac{n}{2}[-\delta - \ln(1 - \delta)]}, \quad (16)$$

where $\delta \geq 0$ is a small value. According to $\ln(1 + \delta) \leq \frac{(2 + \delta)\delta}{2(1 + \delta)}$ and $\ln(1 - \delta) \leq -\delta - \frac{\delta^2}{2}$, we can deduce that:

$$\begin{aligned} P(\|X\|^2 \geq (1 + \delta)n\sigma^2) &= P(Y \geq (1 + \delta)n) \\ &\leq e^{-\frac{n\delta^2}{4(1 + \delta)}} \end{aligned} \quad (17)$$

$$\begin{aligned} P(\|X\|^2 \leq (1 - \delta)n\sigma^2) &= P(Y \leq (1 - \delta)n) \\ &\leq e^{-\frac{n\delta^2}{4}} \\ &\leq e^{-\frac{n\delta^2}{4(1 + \delta)}} \end{aligned} \quad (18)$$

Given the $\sqrt{1 + \delta} \leq 1 + \frac{\delta}{2}$ and $\sqrt{1 - \delta} \geq 1 - \frac{\delta}{2}$, we have:

$$\begin{aligned} P(\|X\| \geq (1 + \frac{\delta}{2})\sqrt{n}\sigma) &\leq P(\|X\| \geq \sqrt{(1 + \delta)}\sqrt{n}\sigma) \\ &\leq e^{-\frac{n\delta^2}{4(1 + \delta)}} \end{aligned} \quad (19)$$

$$\begin{aligned} P(\|X\| \leq (1 - \frac{\delta}{2})\sqrt{n}\sigma) &\leq P(\|X\| \leq \sqrt{(1 - \delta)}\sqrt{n}\sigma) \\ &\leq e^{-\frac{n\delta^2}{4(1 + \delta)}} \end{aligned} \quad (20)$$

Let $\epsilon = \delta/2$, and then organize equations (19) and (20):

$$P(|\|X\| - \sqrt{n}\sigma| \leq \epsilon\sqrt{n}\sigma) \geq 1 - 2e^{-\frac{n\epsilon^2}{1 + 2\epsilon}} \quad (21)$$

which concludes the proof.

The continuous form of (1) can be rewrite as:

$$d\mathbf{x}_t = -\frac{1}{2}g_t^2 \mathbf{x}_t dt + g_t d\mathbf{w}_t, \quad (22)$$

where $g_t^2 = -\frac{1}{\alpha_t} \frac{d\alpha_t}{dt}$. We can use equations (5.50) and (5.51) [67] to derive the relationship between the mean and variance of (22) as they evolve over time:

$$\frac{d\mathbf{m}}{dt} = \mathbb{E} \left[-\frac{1}{2}g_t^2 \mathbf{x}_t \right] = -\frac{1}{2}g_t^2 \mathbf{m} \quad (23)$$

$$\begin{aligned} \frac{d\mathbf{P}}{dt} &= \mathbb{E} \left[-\frac{1}{2}g_t^2 \mathbf{x}_t (\mathbf{x}_t - \mathbf{m})^T \right] + \mathbb{E} \left[-\frac{1}{2}g_t^2 (\mathbf{x}_t - \mathbf{m}) \mathbf{x}_t^T \right] + g_t^2 \mathbf{I} \\ &= -g_t^2 \mathbf{P} + g_t^2 \mathbf{I} \end{aligned} \quad (24)$$

The solutions are:

$$\mathbf{m}(t) = \mathbf{m}(0) e^{-\frac{1}{2} \int_0^t g_s^2 ds} \quad (25)$$

$$\mathbf{P}(t) = \mathbf{I} + (\mathbf{P}(0) - \mathbf{I}) e^{-\int_0^t g_s^2 ds} \quad (26)$$

Since the initial distribution in the latent space is a standard Gaussian distribution, we set $\mathbf{m}(0) = \mathbf{0}$ and $\mathbf{P}(0) = \mathbf{I}$, resulting in:

$$\mathbf{m}(t) = \mathbf{0} \quad (27)$$

$$\mathbf{P}(t) = \mathbf{I} \quad (28)$$

This means that at any given time, the marginal distribution of Stable Diffusion is a standard Gaussian distribution. Combined with Lemma B.1, it follows that \mathcal{M}_t is concentrated on the n -dimensional hypersphere.

C Comparison with Compositional Methods

Compositional generation aims to synthesize complex new samples that simultaneously satisfy multiple attributes or concepts by combining information from multiple different distributions. In the context of diffusion models, this is often achieved by combining the score functions $\nabla_x \log p_t(x)$ of the noise processes from different models to simulate a new reverse stochastic differential equation (SDE).

Du et al. (2023) [61] proposed an energy-based framework for compositional generation, where the scores from multiple models are summed to approximate the score of the joint distribution, that is:

$$\nabla \log p_{\text{PoE}}(x) \approx \sum_{i=1}^N \nabla \log p_i(x),$$

and the corresponding target distribution is the Product of Experts (PoE):

$$p_{\text{PoE}}(x) \propto \prod_{i=1}^N p_i(x).$$

Sampling is performed using MCMC methods such as Langevin dynamics or HMC. However, these approaches are heuristic in nature, lack theoretical guarantees, and incur high computational costs.

Skreta et al. (2025) [66] introduce the *Feynman-Kac Corrector (FKC)* framework, which provides a principled approach to sampling from modified target distributions:

$$\textbf{Annealed: } p_{t,\beta}^{\text{anneal}}(x) = \frac{1}{Z_t(\beta)} q_t(x)^\beta,$$

$$\textbf{Product: } p_t^{\text{prod}}(x) = \frac{1}{Z_t} q_t^1(x) q_t^2(x),$$

$$\textbf{Geometric Avg: } p_{t,\beta}^{\text{geo}}(x) = \frac{1}{Z_t(\beta)} q_t^1(x)^{1-\beta} q_t^2(x)^\beta.$$

They derive weighted SDEs:

$$dx_t = (-f_t(x_t) + \sigma_t^2 \nabla \log p_t(x_t)) dt + \sigma_t dW_t,$$

and apply Sequential Monte Carlo (SMC) to correct sample trajectories. This framework generalizes classifier-free guidance (CFG) and improves inference-time controllability.

Thornton et al. (2025) [65] introduce a novel framework that distills pretrained diffusion models into energy-parameterized models, where the score function is expressed as the gradient of a learned energy $s(x, t) = -\nabla_x E_\theta(x, t)$. To address training instability common in energy-based models, they propose a conservative projection loss that distills the score function from a pretrained teacher model:

$$\min_{\theta} \mathbb{E}_{p_t} [\|\nabla E_\theta(x, t) + s_{\text{teacher}}(x, t)\|^2].$$

This energy formulation enables the definition of new target distributions for sampling. Specifically, in compositional generation tasks, they define a composed distribution as the product of multiple submodels:

$$p(x) \propto \prod_i \exp(-E_i(x)) = \exp\left(-\sum_i E_i(x)\right),$$

which implies that the composed score is equivalent to the sum of individual scores:

$$\nabla \log p(x) = -\sum_i \nabla E_i(x) = \sum_i s_i(x).$$

This resembles the linear score composition used in prior works such as projective composition, but, unlike those methods, which plug the summed scores directly into the reverse diffusion equation.

Bradley et al. (2025) [64] provide a theoretical foundation for *projective composition*. Assuming a *Factorized Conditional* structure, they show:

$$\nabla \log p(x) = \sum_i \nabla_x \log p_i(x) - (k-1) \nabla_x \log p_b(x).$$

where $p_b(x)$ is the background distribution (as in the unconditional model). This combination corresponds to a Bayesian fusion distribution:

$$p(x) \propto \frac{\prod_i p_i(x)}{p_b(x)^{k-1}}$$

This enables direct reverse diffusion sampling without correction under appropriate assumptions. Furthermore, they generalize to feature space combinations, where orthogonal transformations $z = A(x)$ can preserve compositionality.

Based on the above analysis, we first highlight the differences between AMDM and compositional methods to clarify our distinct approach to the task and methodology, details are provided in Table 4.

Table 4: Comparison between AMDM and Composition Methods

Description	AMDM	Composition Methods
Symbol	$p^{\theta_1}(x y), p^{\theta_2}(x y)$ or w/o y	$p^{\theta_1}(x y_1), p^{\theta_2}(x y_2)$ or w/o y_1, y_2
Distribution	Both standard Gaussian distribution	Different data distributions
Condition Input	Same text	Different texts
Output	Within the domain, still a standard Gaussian distribution	Outside the domain, a new distribution such as $p_1 + p_2$ or $p_1 p_2$
Task	Fine-grained generation	Different distribution composition

To further compare the differences in task adaptation, we also provide compositional methods with the same fine-grained input and conduct compositional experiments on both MIGC and InteractDiffusion. The results are compared with the AMDM method and presented in Table 5.

Table 5: Composition of MIGC and InteractDiffusion on the COCO-MIG Benchmark

Method	Instance Success Rate Avg \uparrow	mIoU Score Avg \uparrow	Time (s) \downarrow
Du 2023 [61]	51.29	41.22	42.6
Bradley 2025 [64]	32.74	28.65	12.9
Skreta 2025 [66]	30.21	27.49	11.3
AMDM	54.78	47.74	8.8 (single model 7.5s)

Why dose composition methods performs poorly in fine-grained generation? From equation 4, we observe that the linear combination of different x_t from various models corresponds to the linear combination of their predicted noise, which is proportional to the score. Therefore, the linear combination in AMDM can be interpreted as a linear combination of scores, which is actually similar to the compositional methods. As shown in our aggregation ablation study of AMDM in Figure 5b, linear combination performs worse than spherical aggregation. This is because, in fine-grained generation, the data lies on a spherical manifold, and spherical aggregation better preserves generation quality. Although Du’s method applies Langevin dynamics to improve sample quality after linear aggregation and achieves good results, it comes with substantial computational overhead. Moreover, Bradley’s work theoretically proves that linear score combination only yields high-quality results when the compositional conditions lie in orthogonal feature spaces. However, fine-grained generation typically involves nearly identical conditions, which clearly violates this assumption — providing theoretical support for the observed experimental results. These findings highlight that compositional generation and fine-grained generation are fundamentally different tasks.

Finally, we conduct a simple compositional generation experiment (2D Composition Mixture) to illustrate the limitations of AMDM in compositional generation. The experimental results are shown in Table 6. The reason for the failure of the AMDM algorithm is also quite simple: the distribution is not Gaussian, so AMDM’s spherical aggregation and deviation optimization fail completely.

From above, it is clear that AMDM is fundamentally different from composition methods in both application and algorithmic significance. This paper is the first to propose AMDM, a training-free aggregation algorithm tailored for fine-grained generation, which achieves strong performance without incurring significant computational cost.

Table 6: Comparison of AMDM and Du 2023 under a non-Gaussian distribution

Method	In(MMD) ↓	LL ↑	Var ↓
AMDM	-3.51	-2.43	0.032
Du 2023 [61]	-4.48	1.30	0.007

D Limitations and Broad Impacts

We propose a novel aggregation algorithm AMDM. This algorithm is specifically designed for fine-grained generation tasks using conditional diffusion models, under the constrain that the data distribution follows a normal distribution and the diffusion process are consistent. As demonstrated in the experiments in the Appendix C, AMDM is fundamentally different from previous composition-based generation methods and is tailored for fine-grained generation. Furthermore, we advocate against injecting harmful features into high-quality models to prevent the generation of socially harmful images.

E Additional Visual Results



Figure 6: Additional Visual results of aggregating MIGC into InteractDiffusion applying the AMDM algorithm.



Figure 7: Additional Visual results of aggregating IP-Adapter into InteractDiffusion applying AMDM algorithm.

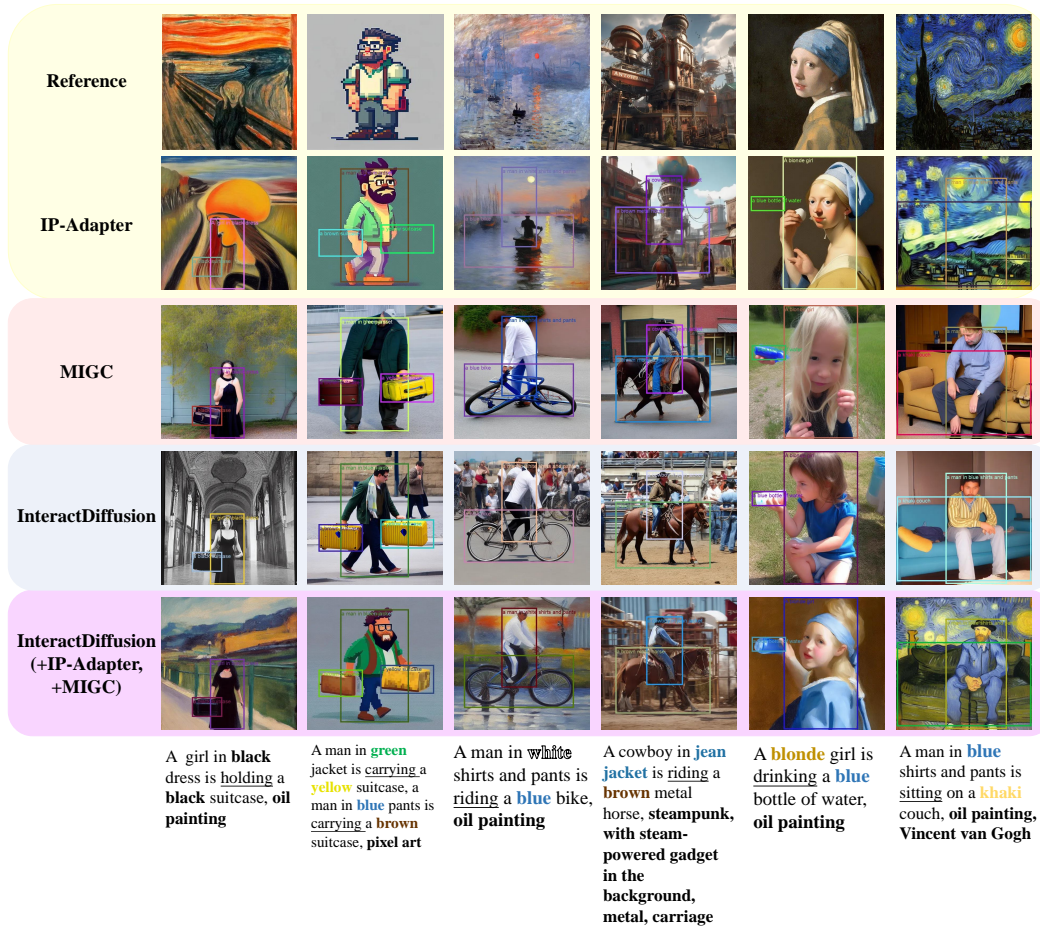


Figure 8: Additional Visual results of aggregating MIGC and IP-Adapter into InteractDiffusion applying the AMDM algorithm.